Progress In Electromagnetics Research, Vol. 127, 537–552, 2012

A NOVEL DUAL-LOOP COUPLER FOR ONE-PORT CYLINDRICAL CAVITY PERMITTIVITY MEASUREMENT

H. Zhang[1], B.-Q. Zeng[1, *], L. Ao[2], and Z. Zhang[2]

[1]National Key Laboratory of Science and Technology on Vacuum Electronics, University of Electronic Science and Technology of China, Chengdu 610054, China

[2]School of Physics Electronics, University of Electronic Science and Technology of China, Chengdu 610054, China

Abstract—The one-port cavity resonator technique based on the S_{11} parameter measurement for measuring the complex permittivity of dielectric samples has been proposed. A novel dual-loop coupler is developed for avoiding and suppressing the spurious modes in one-port cavity resonator. Through threading the pair of half loop in the opposite direction, the opposite surface currents can be generated and only TE_{011} mode will be excited. The operating principles of the dual-loop coupler are investigated. This technique has the advantages of the coupling. Equivalent electronic circuit model has been set up. Simulation and experimental results show good agreement.

1. INTRODUCTION

Application of dielectric materials in the design of microwave components and microelectronics industries requires the exact knowledge of material parameters such as permittivity, conductivity and permeability. Several methods of complex permittivity measurement of dielectrics such as: 1) the free-space technique [1–3] and 2) the transmission measurement technique [4–10] and 3) the cavity perturbation technique [11–13], etc, have been developed in the last several decades. Each of these methods has its own advantages and shortages [14, 15].

Received 26 March 2012, Accepted 28 April 2012, Scheduled 9 May 2012

* Corresponding author: Bao-Qing Zeng (bqzeng@uestc.edu.cn).

The perturbation theory of resonant cavities was first proposed by Bethe and Schwinger [16]. The method is more accurate than the other two techniques (the free-space technique and transmission measurement technique) and has been widely used to study the dielectric and magnetic properties of materials in microwave region, by measuring the shift of resonant frequency and the change in the Q-factor of the cavity when the sample is inserted into the cavity. In this method, the real part of complex permittivity is calculated from the change of the resonant frequency, and the imaginary part is done from the change of Q-factor. The accurate determinations of resonance frequency and Q-factor of the resonators are required.

The circular cylindrical cavity of TE_{011} mode is often applied in this technique. It is important to guarantee that the cavity will have a clear resonant mode. In the conventional cavity, several coupling methods such as: 1) two coupling holes at the upper end plate [17] and 2) two coupling loops in the middle of the cavity wall [18], etc. have been adopted in order to excite the TE_{011} mode. In most of these methods, the grooves, gaps or absorbing materials in the lower end plate of the cavity are introduced to suppress the degenerate TM_{111} mode. The dimensions of the grooves should be calculated exactly and machined accurately. On the other hand, these additional designs may introduce extra errors because of the inflection of the field configurations especially in the region of grooves or gaps.

To solve this problem, we propose a novel dual-loop coupler in TE_{011} cavity as illustrated in Figure 1. The measuring system is designed based on the reflected power technique. Q-factor measurement of one-port microwave resonators employs measurements of the S_{11} parameter as a function of frequency in the method described in presented paper. The coupler consists of two parts: a pair of half circle loops and a joint between them. The currents flowing on the pair of half loops generate fluxes with opposite directions by the Ampere's law. By setting this loop coupler at the desired position, the TM_{111} mode can be suppressed and TE_{011} mode excited in one-port cylindrical cavity. To the best of our knowledge, this kind of coupler has not been applied in measurement.

2. BACKGROUND

2.1. Perturbation Method

For a small dielectric sample of volume V_s (nonmagnetic) inserted in a cavity having volume V_c, the cavity perturbation method gives ε' and

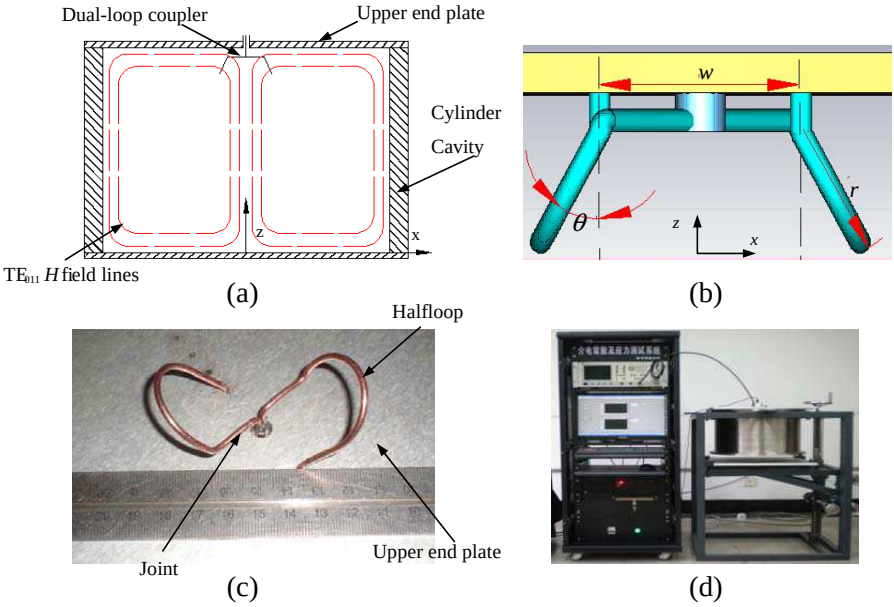

Figure 1. (a) Structure of the resonator. (b) Geometry of dual-loop coupler. (c) Photograph of the dual-loop coupler. (d) Measuring system.

ε'' in terms of the resonance frequency and Q-factor variation [19].

$$\varepsilon' - 1 = \frac{2}{\eta}\frac{f_c - f_s}{f_s} \tag{1}$$

$$\varepsilon'' = \frac{1}{\eta}\left(\frac{1}{Q_s} - \frac{1}{Q_c}\right) \tag{2}$$

where f_c and Q_c are the resonant frequency and quality factor of the empty cavity, respectively, f_s and Q_s are the corresponding quantities in the presence of the dielectric sample. The filling factor η is expressed by

$$\eta = \frac{\int_{V_S}\left|\overrightarrow{E}\right|^2 d\nu}{\int_{V_c}\left|\overrightarrow{E}\right|^2 d\nu} \tag{3}$$

Expressions for dielectric parameters are obtained based on the assumptions [20, 21] that the fields over most of the cavity volume are negligibly changed by the insertion of the sample, and the fields in the sample are uniform over its volume. From the resonance curve, we can obtain the resonance frequency and quality factor.

2.2. Q Measurements of One-port Microwave Resonators

Today the universal instrument for measuring Q factor is automatic network analyzer. In general, the resonance frequency is measured at the minimum or maximum of S_{11} or S_{21}. Q-factor measurements of two-port microwave resonators employ measurement of the transmitted and reflected power as a function of frequency. The scattering parameters at the detuned short position for the circuit shown in Figure 2 are calculated as [22, 23].

$$|s_{11}(\Delta f)|^2 = \frac{(1-\beta_1+\beta_2)^2 + 4\left(\frac{Q_u \Delta f}{f_0}\right)^2}{(1+\beta_1+\beta_2)^2 + 4\left(\frac{Q_u \Delta f}{f_0}\right)^2}. \tag{4}$$

$$|s_{21}(\Delta f)|^2 = \frac{4\beta_1\beta_2}{(1+\beta_1+\beta_2)^2 + 4\left(\frac{Q_u \Delta f}{f_0}\right)^2}. \tag{5}$$

where

$$\beta_1 = \frac{n^2 R_k}{R_s}, \quad \beta_2 = \frac{m^2 R_k}{R_L}.$$

Equation (4) can be applied to one-port resonators if β_2 is set to zero. So we can determine the power reflected from a one-port cavity at the loaded half-bandwidth points $\pm\Delta f_L$ to obtain

$$|s_{11}(\pm\Delta f_L)|\,(\mathrm{dB}) = -3 + 10\log\left(1 + |s_{11}(0)|^2\right). \tag{6}$$

In most cases, the Q-factor can be measured directly by finding out the frequency between 3-dB points of the resonance curve. However, when the sample with high losses is inserted into the cavity, the matched condition of the system will be deeply changed, while the field distribution remains the same. In these cases, we should use (6) to get the value of Q-factor for higher accuracy as illustrated in Figure 3. The key of the problem in perturbation technology is to guarantee that the cavity will have one dominant resonant mode.

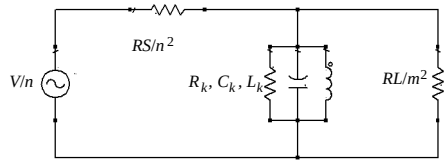

Figure 2. An equivalent LCR circuit for the two ports system [14].

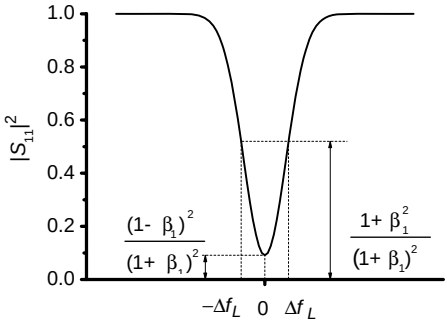

Figure 3. Resonance curve of S_{11}.

3. METHOD

3.1. Coupling Theory of Loop

Condon has given a most convenient theory of the excitation of cavities by loop coupler [24]. In general, a current flowing in the coupled loop will excite all of the cavity modes in varying degree [25]. The resonator has a number of resonant frequencies v_n. An arbitrary field inside the cavity satisfied the boundary conditions can be expanded in terms of the resonant wave normal mode $A_n(\rho)$. It is assumed the loop is small compared to the wave length, that the current distribution in the loop is uniform in our theoretical analysis. So

$$\int A_n(\rho) \cdot ds = \iint curl A_n \cdot dS = M_n. \tag{7}$$

M_n is the flux through the loop of the nth mode. For a unit current, this is then equal to the mutual inductance between the coupling loop and the nth mode. And the impedance of the coupling loop can be calculated

$$Z_{in} = R_0 + j\varpi L_0 + \sum_n \frac{2\pi i \nu M_n^2}{\frac{\pi V}{C^2}\left(\nu_n^2 - \nu^2 + i\frac{\nu\nu_n}{Q_n}\right)}. \tag{8}$$

where V is the volume of the cavity. It should be pointed out that the electric field at the loop coupler is the minimum that corresponds to the point where the input impedance is zero. Hence using (8) in fact shows the impedance of the point about $\lambda/4$ away from the feed point. The distribution of currents on the loop and the direction of the magnetic lines of flux should obey Ampere's circuital law. In the other place the trend of magnetic lines will be governed by the boundary condition of the cavity.

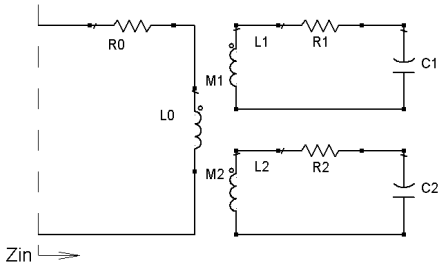

Figure 4. An equivalent LCR circuit for dual-loop coupler.

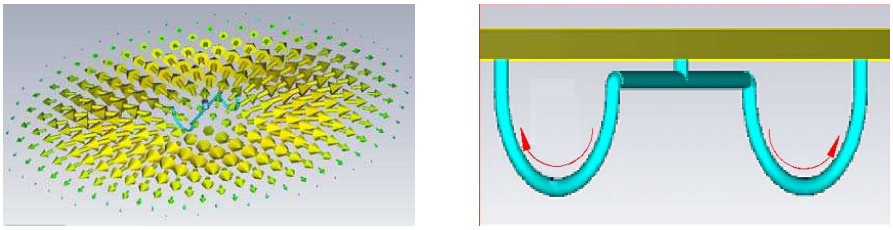

(a) (b)

Figure 5. (a) Simulated TE_{011} H field near the coupler. (b) Simulated TE_{011} surface currents.

3.2. Design

The main problem in the cavity perturbation technique is to suppress the degeneration between TM_{111} and TE_{011} modes. As shown in Figure 1, we apply a novel dual-loop coupler in a cylindrical cavity. The coupler is located at the center of the upper end plate. The pair of half loops, each shorted on its one side, has been associated to a wire fed by a 50 ohm Type-N connector.

From (8), we get an equivalent LCR circuit for the dual-loop coupler as shown in Figure 4. In the vicinity of the TE_{011} mode, the equivalent circuit reduces to two parallel series circuits mutually coupled to the input line. The reference plane of Z_{in} is about $\lambda/4$ away from the feed point. M_1, L_1, R_1 and $C1$ describe the electromagnetism characteristic of a half loop, and M_2, L_2, R_2 and C_2 are about the other. Because of the symmetry of the dual-loop coupler, M_1, L_1, R_1 and C_1 are equal to M_2, L_2, R_2 and C_2 respectively.

If the size of the loop is small compared with a wavelength, the surface currents can be assumed to be equal but with opposite directions on the either loop. The flux lines of TE_{011} magnetic field

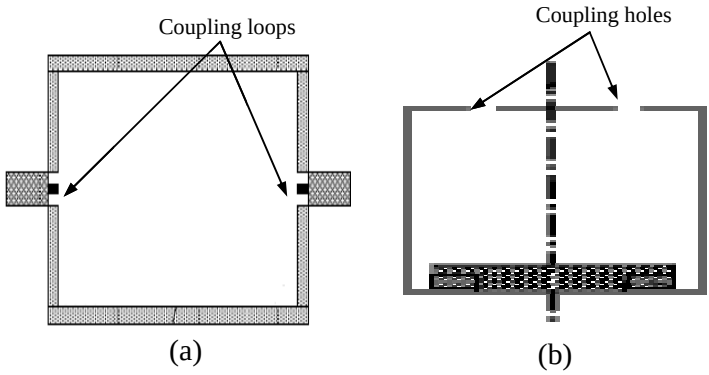

Figure 6. Conventional Coupling methods.

passing through each half loop are in the opposite direction, and accord with the surface currents on both half loops as shown in Figure 5. Supposing the TM_{111} mode can be excited, the flux lines of the magnetic field passing through the each loop will have the same direction, which disaccord with the opposite currents on the both half loops based on Ampere's law. Hence the TM_{111} mode can not be excited.

The conventional coupling methods in the TE_{011} cavity are shown in Figure 6. For case 1 as shown in Figure 6(a), the cavity is coupled with two loops. Compared with the dual-coupler, the coupling loops get closer to a maximum of electrical field. It becomes evident that there will be more extra inflection among the driven loops, field and sample. For case 2 the grooved cavity is used to separate the degeneration between the TM_{111} and TE_{011} modes as shown in Figure 6(b). The groove has to be accurately machined. And these designs may introduce the extra error because of the radiation from the end of the cavity.

4. RESULTS & DISCUSSIONS

4.1. Results

Experiments and simulations have been performed in our system. The radius of the circular cylindrical cavity presented here is 230 mm, and its height is 328 mm. In Figure 7, simulation as well as experimental results are presented and compared. The circles on the $|S_{11}|$ curves represent the resonant frequencies of the cavity.

For the case of only one loop ($r \approx 15$ mm, located at about half

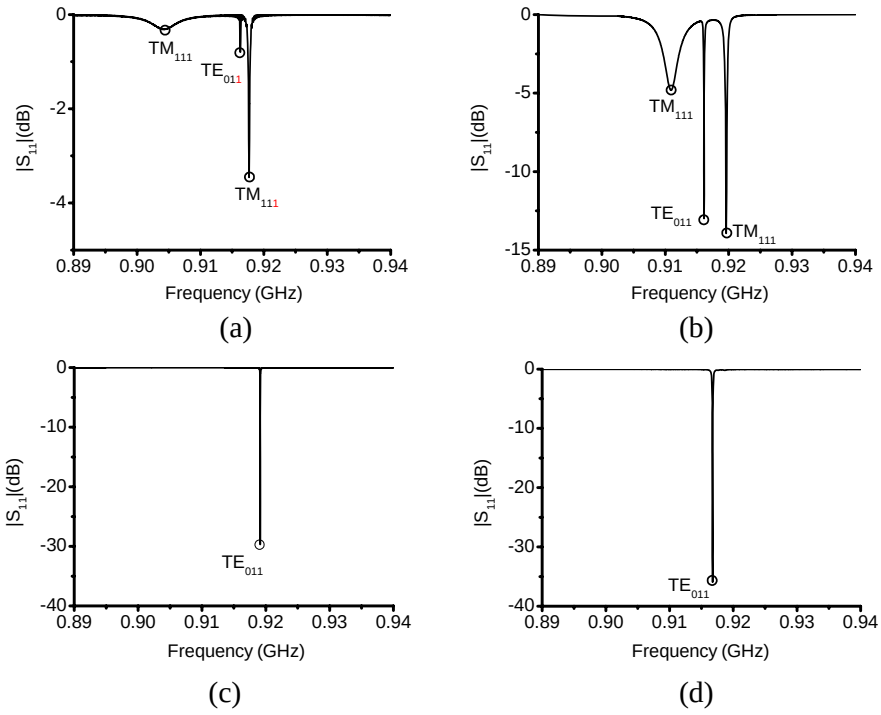

Figure 7. Effect of the dual-loop coupler. (a) Simulated one loop. (b) Measured one loop. (c) Simulated dual-loop. (d) Measured dual-loop.

radius from the axis of the cavity), two TM_{111} polarization degeneracy modes and the TE_{011} mode can been excited altogether as shown in Figures 7(a) and (b). The changes in resonant frequencies due to the perturbations of coupler are different, because of the different field configuration of the two polarization degeneracy TM_{111} modes and TE_{011} mode. Hence the different position of three modes can be understood.

Figures 7(c) and (d) show a comparison between simulations and measurements with a good agreement for the case of dual-loop coupler ($r \approx 15\,\text{mm}$, $w \approx 30\,\text{mm}$, $\theta \approx 40^\circ$). The shape of the $|S_{11}|$ curve shows only one prominent resonance. In a cavity, the Q of the TE_{011} mode is much larger than that of TM_{111} mode. Hence it is easy to distinguish the TE_{011} mode by the way of Q factor. Figure 7(d) shows an optimum example from which the TE_{011} mode resonant frequency and Q factor could be extracted, and thus, ε' and ε'' can be determined using (1), (2). The results of the measurement are tabulated in Table 1.

Table 1. Measurement results.

Sample	f_c (GHz)	f_s (GHz)	Q_c	Q_s	ε'	$\tan\delta$	Published $\tan\delta$
Polyethylene ($t = 40$, $r = 50$)	0.916937500	0.913368750	9975	9728	2.52	0.0002	< 0.0005 [25]
Polyethylene ($t = 35$, $r = 50$)	0.916937500	0.914831250	9975	9755	2.52	0.0003	
Polyethylene ($t = 25$, $r = 50$)	0.916812500	0.914612500	9754	9615	2.50	0.0002	
Nylon6 ($t = 20$, $r = 50$)	0.91691875	0.916637500	9409	8353	3.69	0.0239	0.02–0.03 [25]
Nylon6 ($t = 15$, $r = 50$)	0.916918750	0.916743750	10041	8904	3.67	0.0241	
Nylon6 ($t = 10$, $r = 50$)	0.916906250	0.916806250	10005	9417	3.71	0.0212	
Nylon6 ($t = 5$, $r = 50$)	0.916906250	0.916868750	10005	9788	3.63	0.0191	

(t and r represent the thickness and radius of the sample, unit mm)

4.2. Discussions

In Section 3, the results represent a formal solution to the loop-coupling cavity. Mutual inductance or the magnetic flux through the coupling loop plays an important role in the analysis of the coupling. Hence we set a series of half circular faces parallel to the half loop and calculate the magnetic flux through these faces. Figure 8 illustrates a comparison between simulation and theoretical calculation for the case of dual-loop coupler, where ρ is the distance from the face to the axis of the cavity. The circle on the curve represents the location of the coupler. And the error is due to the local field near the coupler.

Figure 9 shows the local field in the vicinity of the dual-loop coupler. Some of the magnetic flux lines through the coupling loop do not couple with the TE_{011} magnetic field line and only contribute to the self-inductance. This self inductive reactance is the important reason for mismatch and multimode.

To increase our understanding of this coupler, we investigate the dimensions of the loop radius r, space between the two half loops w, and the angle between the loop face and the axis of the cavity θ. We show their influences on resonance curve and field

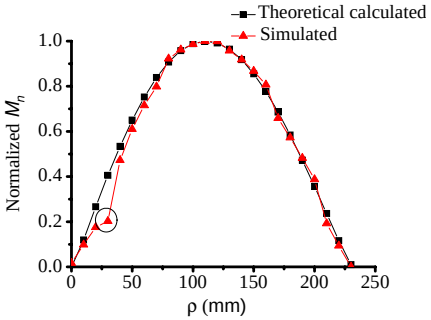

Figure 8. Theoretical calculated and simulated M_n.

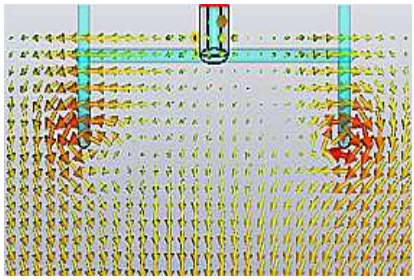

Figure 9. Simulated local field in the vicinity of the dual-loop coupler.

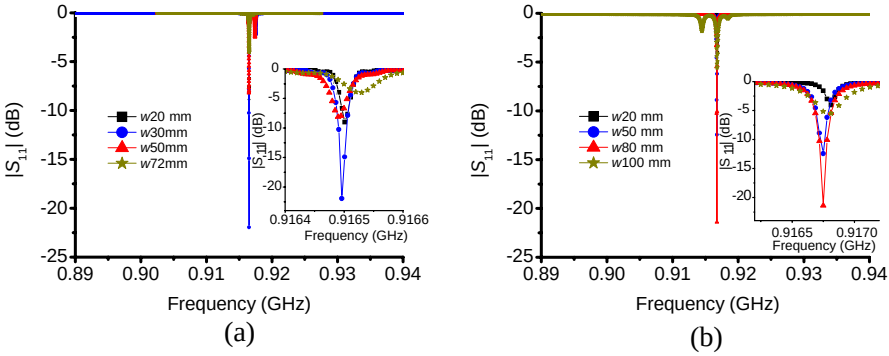

Figure 10. Resonance curve versus w. (a) Simulated results, inset shows the resonance curve between 0.9164–0.9166 GHz. (b) Measured results, the inset shows the resonance curve between 0.9162–0.9172 GHz.

configuration. Varying these parameters thus enables an optimum of M_n by adjusting R to equal the characteristic impedance of the coaxial line and introducing a suitable reactance to tune out the reactance jX.

In Figure 10, we present the magnitude of S_{11} versus w ($r \approx 15\,\text{mm}$, $\theta = 0°$). The shape of $|S_{11}|$ curve shows only one prominent resonance, beside which is a little spurious mode. We can see that w does not have a lot of influence on the location of resonant frequencies. But the resonant amplitude changes obviously. With the increase of w, the resonant amplitude increases at first and then decreases. In Figure 10(a), the simulations show when w is about $0.05\lambda g$, we can obtain a good impedance match. In measurement we often need bigger

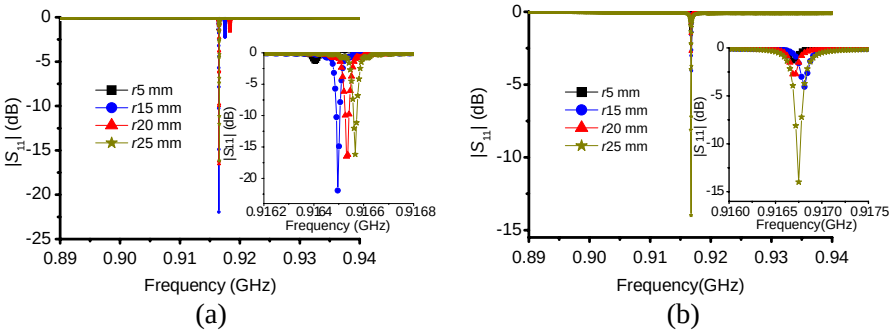

Figure 11. Resonance curve versus r. (a) Simulated results, inset shows the resonance curve between 0.9162–0.9168 GHz. (b) Measured results, the inset shows the resonance curve between 0.9160-0.9175 GHz.

w (about $0.1\lambda g$) maybe because of the conductor loss of the coupler as shown in Figure 10(b). However, with the increase of w, not only the distribution of the surface currents will be more complex, but also the effect of the higher order modes and loss in the coupler become obvious. When $w \approx 100$ mm, the match condition becomes worse and the spurious modes appear. And the trends of the simulation and measurement are consistent and accord with (8).

In Figure 11, we have simulated and measured for different r which varies from 5 mm to 25 mm. ($w \approx 30$ mm, $\theta = 0°$). The shape of $|S_{11}|$ curve is very sensitive to the radius. When the size of the loop is small, r less than $0.1\lambda g$, the currents on the loop can be assumed uniform. The best case is for about 15 mm as shown in Figure 11(a). Meanwhile Figure 11(b) shows in measurement we need larger r just as the situation of w.

When r and w increase, the coupler cannot be looked as a small loop. The relative magnitude of the TM_{111} modes will increase, and their locations in the $|S_{11}|$ curve will change too. The distribution of the surface currents will be more complex and the spurious TM_{111} modes appear.

Figure 12 shows the $|S_{11}|$ curve of a mismatch case ($r = 40$ mm, $w = 76$ mm, $\theta = 0°$). There are three peaks in the $|S_{11}|$ curve, where middle peak is TE_{011} mode and the others are TM_{111} modes.

Figure 13(a) illustrates the magnetic field distribution of the left TM_{111} mode, and the schematic flow of the surface currents on the coupler is shown in Figure 13(b). The magnetic field is mostly due to the z component of the surface currents. The relationship between the

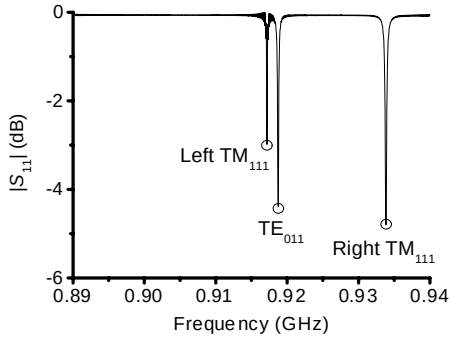

Figure 12. Simulated $|S_{11}|$ of a mismatch and multimode case.

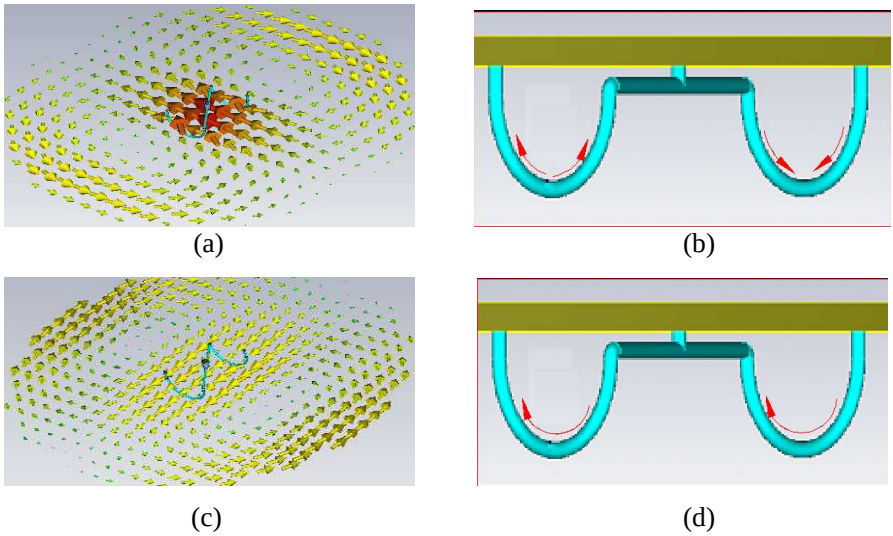

Figure 13. (a) Simulated left TM_{111} mode H field near the coupler. (b) Simulated left TM_{111} surface currents. (c) Simulated right TM_{111} mode H field near the coupler. (d) Simulated right TM_{111} mode surface currents.

current and magnetic field direction obeys the Ampere's circuital law. Either of the half loops becomes the center of the magnetic field.

In Figure 13(c), we present the magnetic field distribution of the right TM_{111} mode. And the surface currents in the coupler have been simulated as shown in Figure 13(d). The currents on the two loops have the same direction, whereas in the TE_{011} mode the currents are

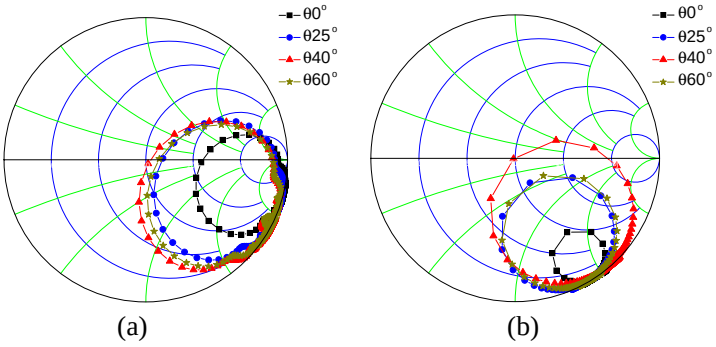

Figure 14. Input impedance versus θ. (a) Simulated results. (b) Measured results.

out of the phase. From these results we can infer that large r or w is not always benefit to excite the TE_{011} mode in the cavity.

In Figure 14, we present the input impedance curve versus θ is present. The angle varies between 0° and 60° ($r \approx 15\,\text{mm}$, $w \approx 30\,\text{mm}$). When $\theta = 0°$, the coupling depends on the radial magnetic field. As the θ increases, the axial flux line can also thread through loops. When the θ adjusts from 0° to 60°, M_n increases at first and has a maximum at about 40°. In this case the magnetic field line almost perpendicularly passes through the loop. The field and currents distribution are unaffected by the presence of the loop. The TM111 mode disappears almost completely.

5. CONCLUSION

Through threading the pair of half loops in the opposite directions, the opposite surface currents on the dual-loop coupler can be generated, and only TE_{011} mode can be excited. Compared with the parameter w and r, θ is easier to tune, which is convenient for us to tune the system. We can first tune the parameters w and r about $0.1\lambda g$ to get a approximate matching, then tune the angle to get exact matching and suppress the spurious mode. Then the resonant frequency and quality factor Q could be extracted from this optimized S_{11} resonance curve of a one-port cavity resonator, and thus, ε' and ε'' can be determined using (1), (2). This method has the advantages of simple setting of the apparatus and fast tuning of the coupling. The error introduced by coupling will be reduced. In the future work, multi-loop coupler and printed technique will be used for better coupling and broadband measurements.

REFERENCES

1. Kim, W. G., N. W. Moon, J. M. Kang, and Y. H. Kim, "Loss measuring of large aperture quasi optics for W-band imaging radiometer system," *Progress In Electromagnetics Research*, Vol. 125, 295–309, 2012.
2. Hasar, U. C. and I. Y. Ozbek, "Complex permittivity determination of lossy materials at millimeter and terahertz frequencies using free-space amplitude measurements," *Journal Electromagnetic Wave and Applications*, Vol. 25, Nos. 14–15, 2100–2109, 2011.
3. Seal, M. D., M. W. Hyde IV, and M. J. Havrilla, "Nondestructive complex permittivity and permeability extraction using a two-layer dual-waveguide probe measurement geometry," *Progress In Electromagnetics Research*, Vol. 123, 123–142, 2012.
4. Hasar, U. C., "Microwave method for thickness-independent permittivity extraction of low-loss dielectric materials from transmission measurements," *Progress In Electromagnetics Research*, Vol. 110, 453–467, 2010.
5. Hasar, U. C., "Procedure for accurate and stable constitutive parameters extraction of materials at microwave frequencies," *Progress In Electromagnetics Research*, Vol. 109, 107–121, 2010.
6. Kadirloglu, F. and U. C. Hasar, "A highly accurate microwave method for permittivity determination using corrected scattering parameter measurements," *Journal Electromagnetic Wave and Applications*, Vol. 24, No. 16, 2179–2189, 2010.
7. Hasar, U. C., "Unique permittivity determination of low-loss dielectric materials from transmission measurements at microwave frequencies," *Progress In Electromagnetics Research*, Vol. 107, 31–46, 2010.
8. Barroso,J. J. and A. L. de Paula, "Retrieval of permittivity and permeability of homogenous materials from scattering parameters," *Journal Electromagnetic Wave and Applications*, Vol. 24, Nos. 11–12, 1563–1574, 2011.
9. Hasar, U. C. and E. A. Oral, "A metric for fast and accurate permittivity determination of low-to-high loss materials from reflection measurements," *Progress In Electromagnetics Research*, Vol. 107, 397–412, 2010.
10. Hasar, U. C. and Y. Kaya, "Reference-independent microwave method for constitutive parameters determination of liquid materials from measured scattering parameters," *Journal Electromagnetic Wave and Applications*, Vol. 25, Nos. 11–12, 1708–1717,

2011.

11. Zhou, Y., E. Li, G. Guo, Y. Gao, and T. Yang, "Broadband complex permittivity measurement of low loss materials over large temperature ranges by stripline resonator cavity using segmentation calculation method," *Progress In Electromagnetics Research*, Vol. 113, 143–160, 2011.
12. Sheen, J., C.-Y. Li, and S.-W. Lin, "Measurements of microwave dielectric properties of (1-x)$TiO_{2-x}$$CaTiO_3$ and (1-x)$TiO_{2-x}$$SrTiO_3$ thin films by the cavity perturbation method," *Journal of Electromagnetic Waves and Applications*, Vol. 25, No. 13, 1886–1894, 2011.
13. Xu, S., L. Yang, L. Huang, and H. S. Chen, "Experimental measurement method to determine the permittivity of extra thin materials using resonant metamaterials," *Progress In Electromagnetics Research*, Vol. 120, 327–337, 2011.
14. Chang, K., *Encyclopedia of RF and Microwave Engineering,* 916–937, Hoboken, N. J., 2005.
15. Deshpande, M. D., C. J. Reddy, P. I. Tiemsin, and R. Cravey, "A new approach to estimate complex permittivity of dielectric materials at microwave frequencies using waveguide measurements," *IEEE Transactions on Microwave Theory and Techniques*, Vol. 45, 359–366, March 1997.
16. Bethe, H. A. and J. Schwinger, "Perturbation theory for cavities," NDRC, Rep, D 1–117, 1943.
17. Li, E., Z. Nie, G. Guo, and Q. Zhang, "Broadband measurements of dielectric properties of low-loss materials at high temperatures using circular cavity method," *Progress In Electromagnetics Research*, Vol. 92, 103–120, 2009.
18. Fang, X., D. Linton, C. Walker, and B. Collins, "A tunable split resonator method for nondestructive permittivity characterization," *IEEE Transactions on Instrumentation and Measurement*, Vol. 53, 1473–1478, December 2004.
19. Altschuler, H. M., *Handbook of Microwave Measurement,* Vol. 2; Sucher, M. and J. Fox, 530, Brooklyn Polytechnic Press, New York, 1963.
20. Kraszewski, A. W. and S. O. Nelson, "Observations on resonant cavity perturbation by dielectric objects," *IEEE Transactions on Microwave Theory and Techniques*, Vol. 40, 151–155, January 1992.
21. Carter, R. G., "Accuracy of microwave cavity perturbation measurements," *IEEE Transactions on Microwave Theory and*

Techniques, Vol. 49, 918–923, May 2001.

22. Galani, Z., M. J. Bianchini, R. C. Waterman, R. Dibiase, R. W. Laton, and J. B. Cole, "Analysis and design of a single resonator GaAs FET oscillator with noise generation," *IEEE Transactions on Microwave Theory and Techniques*, Vol. 32, 1556–1565, 1984.
23. Han, D. H., Y. S. Kim, and M. Kwon, "Two port cavity Q measurement using scattering parameters," *Rev. Sci. Instrum.*, Vol. 67, 2179–2181, 1996.
24. Condon, E. U., "Forced oscillations in cavity resonators," *Journal of Applied Physics*, Vol. 12, 129–132, February 1941.
25. Jakes, Jr., W. C., "Analysis of coupling loops in waveguide and application to the design of a diode switch," *IEEE Transactions on Microwave Theory and Techniques*, Vol. 14, 189–200, April 1996.
26. Dean, J. A., *Lange's Handbook of Chemistry,* 15th Edition, McGraw-Hill, New York, St. Louis, San Francisco, Auckland, Bogota, Caracus, Lisbon, London, Madrid, Mexico, Milan, Montreal, New Delhi, Paris, San Juan, Sao Paulo, Singapore, Sydeny, Tokyo, Toronto, 1998.